Functional-Graded Index Metasurfaces for Infrared Radiation and Guiding

Mohsen Farmahini-Farahani, *Student Member, IEEE*, and Hossein Mosallaei, *Senior Member, IEEE*

***Abstract*—We present the fundamental principle of plasmonic-graded-index materials for radiating and guiding at infrared range. The method to derive effective refractive index is presented and effective refractive index engineering is comprehensively investigated by obtaining complex dispersion diagrams. As an illustrative example for radiating structure, a graded index metasurface is designed for collimating the power emanating from an aperture to a steered narrow beam. The center frequency of operation is 57.5 THz. The half power beam widths of the beam radiated from a $15\lambda \times 15\lambda$ metasurface to $\theta = 30°$ direction are 6° and 16° in elevation and azimuth planes, respectively. Radiation efficiency is calculated to be 86%. To demonstrate the guiding application, a flat step index waveguide is designed. The surface wave guiding is characterized by obtaining complex dispersion diagram and mode profiles. The applications of such waveguides in feeding antennas and routing surface waves are demonstrated with some unique designs.**

***Index Terms*—Graded index, hologram, metasurface, plasmonics.**

I. Introduction

GRADED index optical materials, materials with gradual change in refractive index, have introduced a new degree of freedom for designing optical devices. Previously, simple index contrast (step index fibers) and geometrical curvature (lenses) were the main design parameters for optical devices. In graded index materials, however, the refractive index profile determines the light rays trace inside the material. Such designer materials are used to realize flat optical devices such as lenses for many applications, for instance, focusing, imaging, and routing. Conventional-graded index materials are produced with an ion exchange method when diffusion is engineered to manipulate refractive index. Metamaterial-graded index structures are realized by introducing subwavelength diffractive elements such as holes and gratings into the bulk of dielectric material [1]–[4]. Since the inclusions are subwavelength, the effective index can be used to characterize the artificial medium.

Recently, the high demand for miniaturized photonic-integrated circuits has brought a lot of attentions to plasmonic devices. Subwavelength plasmonic particles can interact with light and manipulate light intensity, phase or polarization state. Several planar plasmonic devices are reported for beam focusing and steering applications at infrared and visible range [5]–[11]. These planar surfaces work as transmit or reflect arrays and essentially function as metalenses. One approach to describe the effect of these patterned plasmonic particles in the context of optical devices is to use well-known refractive index terminology. Even, the term "generalized laws of reflection and refraction" is used to describe the effect of patterned plasmonic particles on a surface [8].

Flat optics or optics on the surface using surface plasmons has emerged as a promising solution for photonic-integrated circuits [12]–[15]. Use of plasmonic particles can revolutionize refractive index engineering since a variety of index profiles can be designed merely with patterning metals on top of dielectrics. For instance, numerical simulation has shown graphene layers with patterned conductivity for focusing and Fourier optics applications [14]. Also, a surface patterned with H-shaped plasmonic particles is shown to link surface waves to propagating waves [15]. The promises of plasmonic-graded index material include low profile, ease of fabrication, and enhanced optical devices.

Here, we are employing effective refractive index concept to realize desired index profiles using metallic nanostructures. First, we comprehensively explore the effective index manipulation using plasmonic particles. Then, we design some plasmonic-graded index devices to show the versatility of our approach. We use holography theorem to devise an INFRARED planar-graded index hologram integrated into an aperture for beam forming applications. Metallic patches are used to manipulate the refractive index of the surface around the aperture. The loss and bandwidth performance of such metasurfaces are investigated.

Also, we show INFRARED metasurface patterns that confine and guide a wave on the surface based on index contrast. The waveguide is essentially a flat fiber optics working based on total internal reflection phenomena. The index of the surface is graded accordingly with plasmonic particles. Propagation properties of such surface waveguides are investigated as well.

The paper is organized as follows. In Section II, we show how to obtain effective refractive index of a unit cell of plasmonic particles. We thoroughly investigate the parameters controlling the effective index. In Section III, we present a graded index hologram for beam forming application. In Section IV, we focus on confining traveling surface waves in a surface waveguide using effective index engineering.

II. Artificial Plasmonic-Graded Index Material

The refractive index can be manipulated using subwavelength building blocks (plasmonic scatterers or nanoantennas [16]) to

Manuscript received April 4, 2014; revised August 31, 2014; accepted October 20, 2014. Date of publication October 31, 2014; date of current version January 6, 2015. The review of this paper was arranged by Associate Editor M. De Vittorio. This work was supported in part by the U.S. Air Force Office of Scientific Research and the U.S. Office of Naval Research. Also, performing simulations was possible at the Center for Nanoscale System Clusters, Harvard University, a Member of the National Nanotechnology Infrastructure Network, which is supported by the National Science Foundation.

The authors are with the Department of Electrical and Computer Engineering, Northeastern University, Boston, MA 02115 USA (e-mail: farahani@ece.neu.edu; hosseinm@ece.neu.edu).

Color versions of one or more of the figures in this paper are available online at http://ieeexplore.ieee.org.

Digital Object Identifier 10.1109/TNANO.2014.2365554

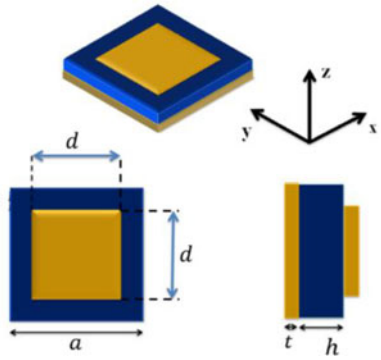

Fig. 1. Unit cell of the metallic patch on a grounded substrate. The effective index can be manipulated by changing substrate material and thickness as well as the patch size.

provide a fine, yet physically realizable resolution for effective index approximation. The metallic particles interact with the surface wave and decrease wave velocity.

We chose square metal patches on a dielectric substrate backed with a metal as building blocks for effective index engineering (see Fig. 1).

In a conventional dielectric slab waveguide, the effective index depends on center dielectric thickness and the materials index. Here, effective index is dependent on the patch size as well. So, instead of changing thickness or material, one can simply pattern the patch dimension as desired. This approach offers a huge simplicity advantage from fabrication standpoint.

The effective index is calculated from dispersion diagram of a guiding structure from (1).

$$n_{\text{eff}} = \frac{k_t}{k_0} \tag{1}$$

where k_t and k_0 are guided and free space propagation constants. The dispersion diagrams of 2-D dielectric slabs are simply obtainable in the form of transcendent equations. However, one need to use numerical techniques for more complex structures which involve metals with Drude model at infrared frequency to precisely calculate propagation characteristics.

The dispersion diagram of patch building blocks can be calculated assuming local periodicity. We use 3-D FDTD solver from Lumerical Inc. [17] to obtain the dispersion diagram of a square metal patch unit cell (see Fig. 1) in 45–70 THz band (4.3–6.7 μm). The Bloch and periodic boundary conditions are applied in x- and y-directions, respectively. Perfectly matched layer (PML) is used for boundary in z-direction. The PML layer distance is set to avoid any power loss in the PML layer. Metal patch and substrate back metal are made from gold. The gold Palik model from Lumerical material library is used for simulation ($n_{\text{Au}} = 4.4 + i33.4$ @55 THz). The substrate is SiO_2 with refractive index (n) of 1.35 at the desired band. The substrate and gold layer thickness are 300 and 50 nm, respectively.

First, we investigate the effect of patch size (d) on the effective index. The fundamental mode calculated here is a TM mode with E_x, E_z, and H_y components (x is the propagation direction). The dispersion diagram for different patch sizes is depicted

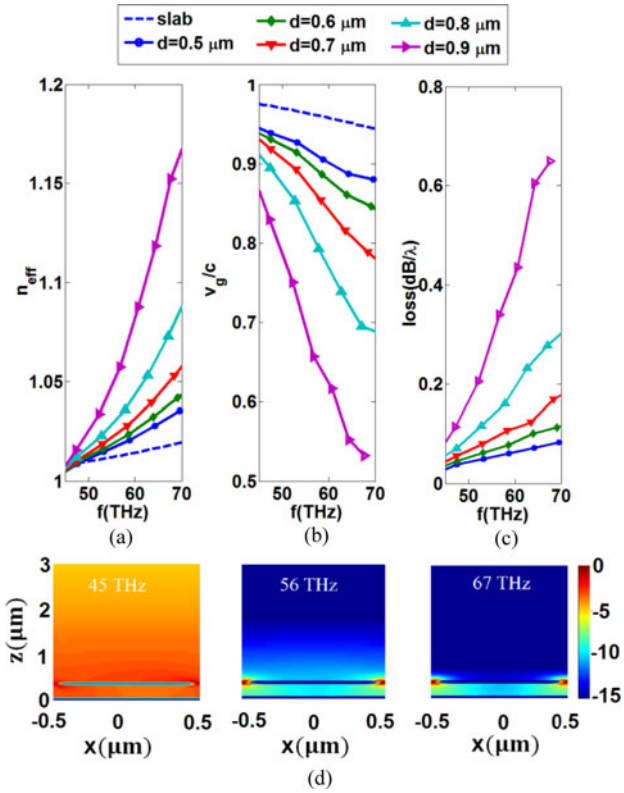

Fig. 2. (a) Dispersion diagram. (b) Normalized group velocity. (c) Loss diagram of the unit cell for different patch sizes and a dielectric slab waveguide. (d) Intensity (dB) of electric field distribution at three different frequencies depicting loosely and tightly bounded surface waves.

in Fig. 2(a). The dispersion diagram of a dielectric slab with thickness of 300 nm is also depicted in the same graph. As shown, the effective index of the plasmonic unit cell changes sharply compared to the dielectric slab. Therefore, it is possible to achieve the desired index at the frequency range of interest and skip the limitations of an all-dielectric slab. This occurs at the expense of higher propagation loss as clear from Fig. 2(c). Also, the larger the patch, the sharper are the index variations. Fig. 2(b) depicts the normalized group velocity of the wave in the unit cell compared with the dielectric slab case. The group velocity is the energy travel velocity and indicates density of a dielectric. One can observe slow wave propagation in the plasmonic patch unit cells.

Note that a frequency nondispersive waveguide has a constant effective index over frequency. Therefore, frequency dispersion of the plasmonic unit cell is much higher compared to the ordinary slab waveguide and this limits the operation bandwidth of the devices with plasmonic graded index building blocks.

The intensity of electric field is shown at three frequencies on the dispersion diagram. The electric field intensity is higher at the gap between the two unit cells. At lower frequencies, the field is loosely bounded to the surface and extends into free space while at higher frequency the field is tightly bounded to the surface. Expectedly, at higher index of refractions, the field is more confined to the substrate and metal gap. This will result in increased propagation loss. The loss diagram depicted

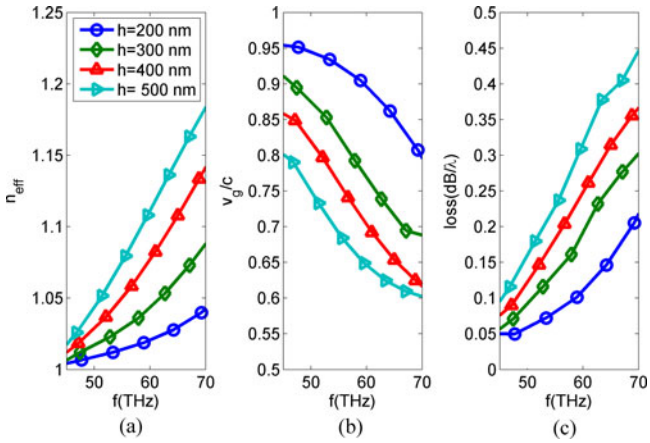

Fig. 3. (a) Dispersion diagram. (b) Normalized group velocity. (c) Loss diagram of the unit cell of 800 nm patch on top of SiO2 with thickness (h) sweeping from 200 to 500 nm. Thicker substrates increase effective refractive index at the expense of higher loss.

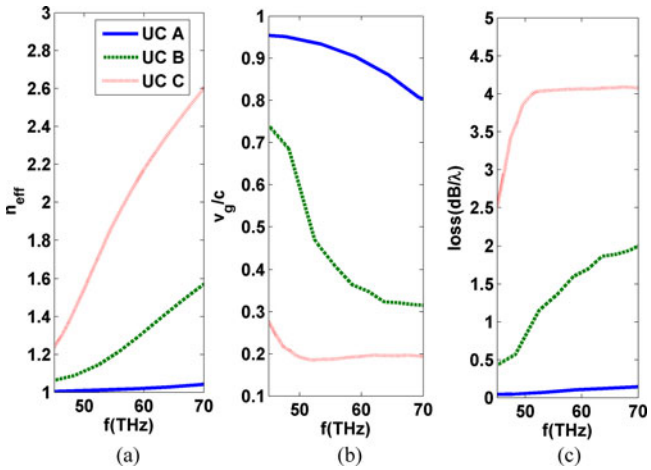

Fig. 4. (a) Dispersion diagram. (b) Normalized group velocity. (c) Loss diagram for three unit cells with different dielectrics. The refractive index of unit cell A, B, and C are 1.35, 2, and 3, respectively. One need to choose proper dielectric to obtain the desired refractive index; however, higher values of n are obtained at the expense of more loss.

in Fig. 2(c) confirms this statement. It should be noted that larger patches incur more propagation loss.

We further investigate the effect of dielectric substrate refractive index and thickness on the effective refractive index of the unit cells. We evaluate the range of available effective indices obtainable with a plasmonic inclusion.

First, we change the substrate thickness. We use the same unit cell parameters as before. The patch size is fixed to 0.8 μm and the thickness is swept from 200 to 500 nm. From dielectric slab theory, we expect higher values for refractive index as we increase the thickness. Our simulation confirms this as shown in Fig. 3. For instance, the value of refractive index increases from 1.04 to 1.19 as we increase the thickness from 200 to 500 nm at 70 THz. As a result, according to the required range of refractive index, one must choose proper substrate thickness. Note that higher values of refractive index mean more confined waves and extra metal loss.

Substrate refractive index considerably affects the effective index. To show this effect, we simulate three different unit cells as follows: unit cell A: $a = 1000$ nm, $n = 1.35$, unit cell B: $a = 800$ nm, $n = 2$ and unit cell C: $a = 700$ nm, $n = 3$. In all cases, the gap size (a–d) is 0.2 μm (The patch size is 900, 700, and 500 nm, respectively). The unit cell size is determined to keep the effective patch length (physical length divided by n) fixed. Also, the substrate thickness is 200 nm for all unit cells. The result of this set of simulation is shown in Fig. 4. Expectedly, unit cell C has higher effective index because of substrate higher index. One can observe three different regions in the dispersion diagrams shown in Fig. 4. These regions are more obvious in group velocity or loss diagrams. For unit cell A, group velocity slightly decreases with frequency and propagation loss goes up subtly. In unit cell B case, there is a sudden drop in group velocity and at the same time the propagation loss plummets. In unit cell C, the group velocity reaches to its minimum and stays there while the loss is almost constant.

These curves reveal very useful information about the range of available refractive indices for different materials and the associated propagation loss. For instance, one would infer high effective index of 2 is obtained with $n = 3$ at the expense of intolerable loss. Therefore, using plasmonic particles with high index materials is not a reasonable solution because of extra loss. One should adopt other solutions such as using grating, holes or composite of high index and low index material as illustrated in [2], [4] and [18].

Finally, we observe the effect of cell size on the effective index. Here, we choose $a = 1$ μm, 0.9, and 0.8 μm with substrate a 200-nm-thick SiO_2. The simulation results show that the important parameter determining n is gap size rather than unit cell size. For instance, a 800-nm patch in a unit cell of 1 μm (gap size 200 nm) offers smaller effective index than a 800-nm patch in a 900-nm unit cell (gap size 100 nm).

Considering the curves offered in this section, one can generally associate higher effective index values with higher metal loss. Therefore, the operation frequency must be chosen to avoid working in the tightly bounded part of the dispersion diagram where metal loss is intolerable.

III. Graded Index Surfaces for Radiation

Optical antennas are required for efficient coupling of optical power into free space or the numerical aperture of optical fibers. An optical antenna radiates source power into free space in a desired direction. Use of leaky wave antennas and holograms in Gigahertz range have shown to be promising antenna solutions for applications requiring high gain from a flat antenna [19], [20]. Optical leaky wave antenna is also proposed for beam collimation applications. A Si-based optical leaky wave antenna is working at 1550 nm investigated in [18]. A Si slab ($n = 3.4$) that is periodically perturbed with Si_3N_4 ($n = 1.67$) to excite leaky mode. Here, we use holography design technique to obtain a graded index hologram operating as an optical antenna.

The main idea of holography is to produce a desired output wave function from scattering of a known input wave function

with a designed hologram. The function describing the profile of the hologram is obtained based on the interference pattern of the known input and the desired output wave functions. We may modify a surface to represent the function of the hologram by manipulating some quantity related to the surface such as its refractive index. Suppose, we start with a desired output beam and a known input source as wave functions, $\Psi_{\rm in}$ and $\Psi_{\rm out}$. The interference pattern (hologram) is then proportional to $\Psi_{\rm out}\Psi_{\rm in}^{*}$ [19], [21].

Imagine if one is interested to calculate a hologram pattern that transforms a surface wave emanating from a point source into a pencil beam at the direction defined by θ_0 and φ_0 in the spherical coordinate system. Then, the input scalar wave function is proportional to

$$\Psi_{\rm in} \propto \exp(-jk_0 n_{\rm eq}\rho) \tag{2}$$

where k_0 is the free space wave number, $n_{\rm eq}$ is the equivalent refractive index of the surface and ρ is the radial distance from the center. The desired output beam is a pencil beam at the direction defined by θ_0 and φ_0. As a result, the output wave function is $\Psi_{\rm out} \propto \exp(-jC(\rho,\varphi))$ where phase distribution is given by

$$C(\rho,\varphi) = k_0\rho\sin\theta_0\cos(\varphi-\varphi_0). \tag{3}$$

Here, φ is the azimuthal component of the cylindrical coordinate system. The hologram effective index should be proportional to the interference pattern of input and output wave functions. Then, one can obtain the required refractive index profile

$$n(\rho,\varphi) = n_0\{1 + n_M\cos(k_0\rho(\sin\theta_0\cos(\varphi-\varphi_0) - n_{\rm eq}))\} \tag{4}$$

where n_0 is the mean value and n_M is the modulating factor incorporated to span the whole range of available effective index. This relation is similar to the one for sinusoidal-modulated reactance surfaces analyzed in [22] for 1-D cases. Likewise, one can deduct that higher index variations, larger (smaller) n_M, causes faster (slower) leakage of the surface wave into free space, smaller (larger) antenna size and wider (narrower) beamwidth.

As shown in Fig. 2(a), effective refractive index can be modulated with varying the patch sizes. We can realize the effective index profile in (4) with varying patch sizes according to the data provided in Fig. 2(a). Fig. 5 shows the effective index versus patch size obtained from Fig. 1(a) at 57.5 THz. The mean value ($n_0 = 1.053$) and modulating factor ($n_M = 0.032$) are obtained from the maximum and minimum achievable effective index.

To demonstrate the suggested design scheme, we investigate a hologram to collimate the radiated beam of an aperture into a narrow steered beam with $\theta_0 = 30°$ and $\varphi_0 = 0°$. The design frequency is 57.5 THz. The refractive index profile is obtained from (4) and transformed to patch size profile using Fig. 5. The resulting graded index hologram pattern is depicted in Fig. 6(a). The hologram size is $78\,\mu\text{m} \times 78\ \mu\text{m}$. It is excited from a $3\,\mu\text{m} \times 2\ \mu\text{m}$ aperture at the center. The aperture is the open end of a rectangular waveguide extended into the ground. The structure is simulated in Lumerical and the results

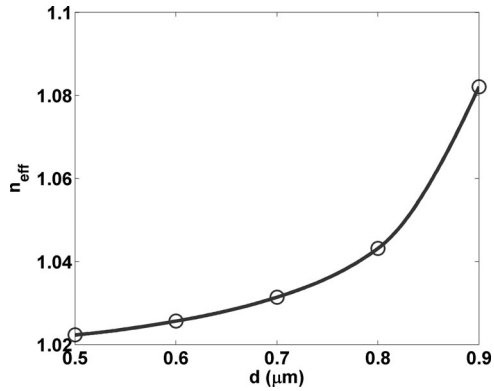

Fig. 5. Variations of effective index versus patch size for the unit cell of Fig. 2 at 57.5 THz. As expected, effective index is larger for larger patch sizes.

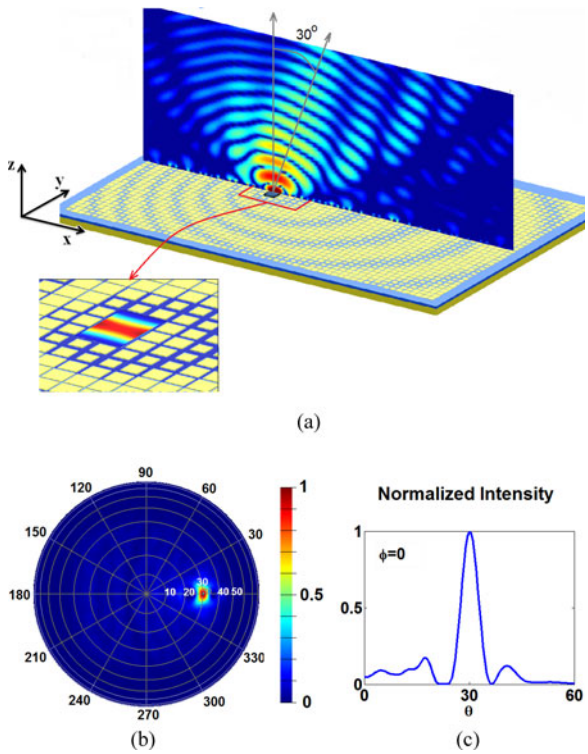

Fig. 6. (a) Hologram (not to scale) patterning the aperture and the near filed electric field intensity illustrating beam steering. The inset shows the field intensity at the aperture. (b) Simulated 2-D farfield radiation from the graded index hologram. The beam is steered into $\theta_0 = 30°$ and $\varphi_0 = 0°$. (c) $\varphi_0 = 0°$ cut of the farfield pattern in (b). The HPBW is 6°.

are presented in Fig. 6. The PML boundary conditions are placed around the structure to allow for radiation. The top PML layer is two wavelengths away from the structure and the side PML layers are half wavelength away.

The intensity distribution of the aperture is shown in the inset of Fig. 6(a). A 2-D cut of the electric field is overlaid on hologram in Fig. 6(a). As illustrated, the power emanating from the aperture propagates along the surface and leaks into free space radiation mode. The main beam is directed to 30° as designed. The other beams are for higher order radiations

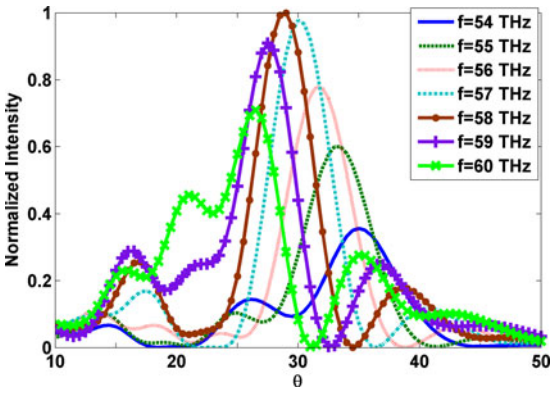

Fig. 7. Farfield intensity versus θ at different frequencies. From 55 to 60 THz, the half power bandwidth is 8.7%.

which are not carrying considerable power. Fig. 6(b) depicts the simulated 2-D far-field intensity of the graded index hologram radiation. As expected, the hologram has collimated the surface wave coupling from the aperture to a narrow concentrated beam in 30° [See Fig. 6(c)]. The HPBW is 6° and 16° in elevation and azimuth directions, respectively.

To explore the bandwidth performance of the designed beam former, we obtain the farfield at frequency range of 54–60 THz. As expected, the beam peak steers away from 30° at other frequencies and the amplitude also drops. Fig. 7 shows the farfield-normalized intensity at different frequencies. As depicted, the half power intensity band width is 55–60 THz (8.7%). Also, the beam steers from 26.5° to 33.5° at this frequency range.

We also calculate the injected power from the aperture to the surface wave, the radiated power and the power absorbed in metal at the design frequency, 57.5 THz.

The radiation efficiency defined as the ratio of the radiated power to the injected power and total efficiency is the ratio of the radiated power to the source power. The difference between the source power and injected power is the power reflected back to the source because of mismatch. Our simulation has shown that only 2% of the source power reflects back. Hence, radiation efficiency and total efficiency are very close. Simulation results show that 86% of the source power radiates away from the metasurface.

We note an important design consideration here. According to the dispersion curves in Fig. 2, the variation of the effective index is small and loss is negligible at low frequency part of the dispersion curves. On high frequency part of the curves, the variation on the effective index is large and loss is not negligible. A design at low frequency part will be low loss, but with small modulation factor n_M. The surface wave will leak into free space very slowly and a large hologram is required. On the other hand, the design at high frequencies will result in increased metal loss but a faster leakage into free space which does not require a large hologram. The tradeoff between metal loss, modulation factor should be carefully considered in the design procedure. The unit cells size can be tuned to obtain the required modulation factor and loss at the desired frequency. Also, the aperture can be the opening of a quantum cascade laser.

IV. Flat-Graded Index Waveguides

Engineering refractive index of materials has been used to realize waveguiding structures such as ridge waveguides and fiber optics [23]–[25]. Index contrast between core and cladding causes field confinement and propagation. Analytical methods based on geometric optics and wave equations for simple geometries and numerical methods for more complex geometries are employed to characterize such waveguides. While optical fiber are mainly used for transmission over long range distances, the ridge waveguides are used for light routing in flat photonic circuits.

In Section II, we illustrated how a desired refractive index profile can be obtained using plasmonic patches. We can use the elements now to design an infrared surface waveguiding. The interface of plasmonic and dielectric materials supports surface plasmon polaritons. One can use the engineered effective index contrast to confine the surface wave in lateral dimension as well. A high index metasurface is sandwiched between two low index metasurfaces to realize a step index flat waveguide [See Fig. 8(a)]. The high index area is patterned with larger patches and the low index area with smaller ones. The principle of operation is similar to dielectric slab waveguides. Such surface waveguide strategy was studied originally in GHz [26], [27]. Here, we implement it in INFRARED considering the actual material property for elements and to investigate the performance and loss in great depth.

As an example, we design a waveguide with the following dimensions: high index area width (w_1): 5 μm, patch length: 0.9 μm, low index area width (w_2): 5 μm, patch length: 0.5 μm, substrate: 300-nm-thick SiO_2 [See Fig. 8(a)]. We obtain the dispersion diagram for the TM mode propagating in the waveguide using Lumerical.

Fig. 8(b) and (c) shows the field profile of the TM mode propagating in the step index flat waveguide. The wave is confined in the high index area as shown in the field profiles. Note that the power mainly concentrated in the gap between patches.

Note that in Fig. 8(c), the waveguide touches PML layer. Since the materials are dispersive, the simulation is prone to instability. Reducing the dt stability factor can overcome this problem.

Fig. 8(d) depicts waveguide effective index. The wave is guided as a slow wave inside the high index region as group velocity is depicted in Fig. 8(e). Finally, the propagation loss is presented in Fig. 8(f). One can observe the propagation loss from Fig. 8(c) where the intensity of the electric field decreases along propagation direction. We place power monitors at two positions 45 μm (9λ at 60 THz) apart. The intensity drops 4.5 dB; hence, the propagation length of the step index waveguide is nine times the wavelength at 60 THz. This value is consistent with the loss diagram depicted in Fig. 8(f). The effective index is 1.1 and the group velocity is almost half of the speed of light.

As next design we investigate a new way to efficiently launch hologram metasurfaces using the proposed waveguide. The excitation scheme is illustrated in Fig. 9(a). We design a step index waveguide and then merge it to the side of the hologram surface. The hologram is tapered accordingly to fit the waveguide lateral

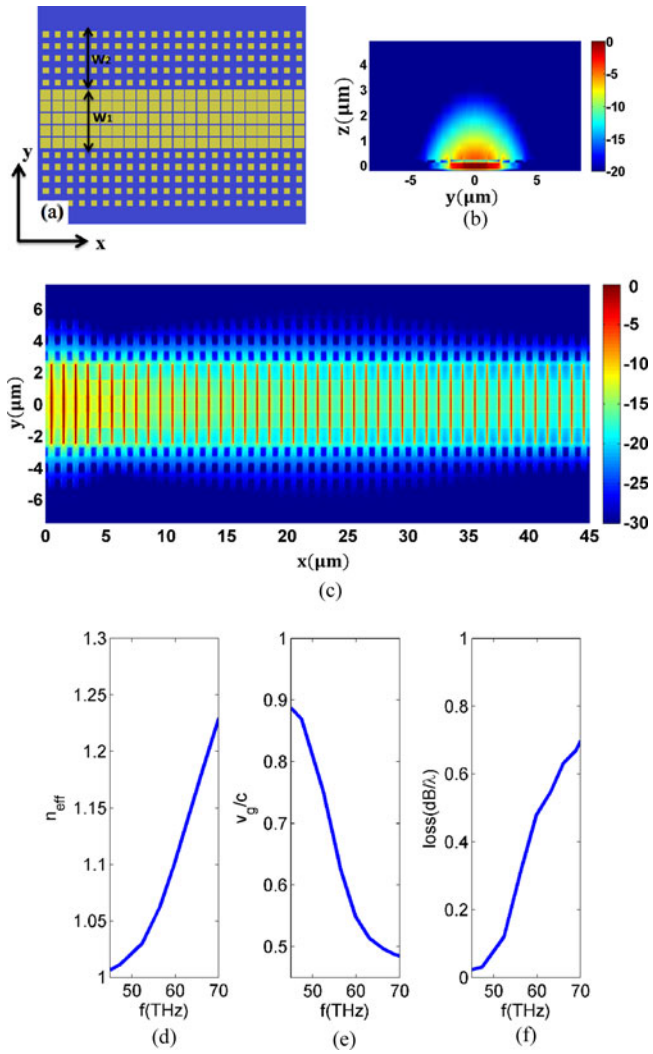

Fig. 8. (a) Step index flat waveguide with $w_1 = 5$ μm, $w_2 = 5$ μm. (b) TM mode electric field intensity profile at 60 THz. (c) Lateral confinement of the energy in high index area at $z = 150$ nm. (d) Dispersion diagram. (e) Normalized group velocity. (f) Loss diagram of a step index flat waveguide with $w_1 = 5$ μm, $w_2 = 5$ μm. The patch size is 0.9 μm for the high index region and 0.5 μm for low index region.

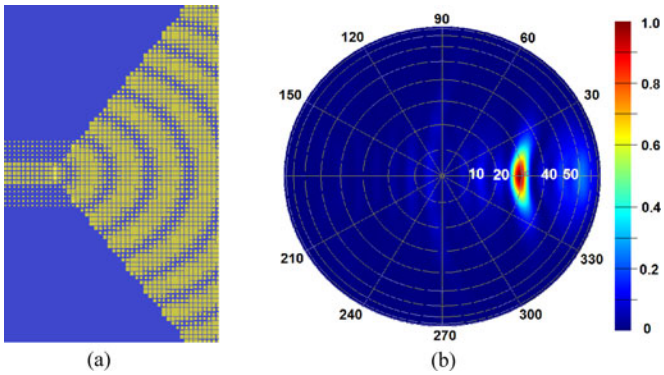

Fig. 9 (a) Step index flat waveguide used to feed a metasurface hologram. The hologram size is $36\,\mu\text{m} \times 72$ μm and the taper angle is 51°. (b) Farfield radiation of the structure at 58 THz. The hologram has collimated the beam into 29°. The vertical HPBW remains the same as Fig. 6 but the lateral HPBW increase to 31° because of the tapering.

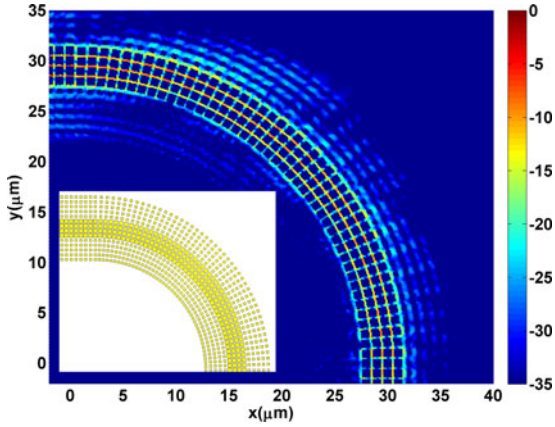

Fig. 10 Filed intensity (dB) profile on the surface of SiO_2 ($z = 150$ nm). The bending of the beam is realized. The bend incur 1.3 dB extra loss as a result of leakage. The inset shows the structure of the bend designed to rotate the surface wave by 90°.

dimension. The hologram size is $36\,\mu\text{m} \times 72$ μm and the taper angle is 51°.

The waveguide has the same dimension of the one analyzed in Fig. 8. It is excited with the dominant mode at 58 THz and the farfield is calculated accordingly. Fig. 9(b) shows the farfield intensity.

The hologram has steered the beam into 29°. The vertical HPBW remains the same as Fig. 6, i.e., 6°, but the lateral HPBW increase to 31° because of the tapering. This illustrates a very novel approach to launching holograms in a 2-D-integrated system approach.

Finally, we design a bend with the introduced waveguide to demonstrate routing of the waves on the surface. This time we excite the TE mode of the waveguide. Note that the ground is removed to enable TE mode propagation. We use a waveguide with following dimensions: high index area width (w_1): 4 μm, patch length: 0.9 μm, low index area width (w_2): 5 μm, patch length: 0.5 μm, substrate: 300-nm-thick SiO_2.

The outer waves in a bend travel longer distances compared to the inner waves. This will distort the phase front. Therefore, we should determine the effective index to compensate for the different propagation lengths. If we change the effective index proportional to the inverse of radius, we can guarantee an undistorted phase front. Therefore, the patch size in the inner part of the bend is larger compared to the outer parts.

The bend radius is selected to be equal to 25 μm (5λ) and the gap sizes are determined accordingly. The bend length is 39 μm. This length will induce a propagation loss of 4.3 dB. The inset in Fig. 10 depicts the structure of the bend realized using the metallic patches. This structure is simulated in Lumerical and the field intensity profile is obtained. As shown in Fig. 10, the bend actually rotates the wave propagation direction by 90°. The leakage is small, however, it causes extra loss. The calculated loss is 5.7 dB. Therefore, 1.3 dB loss is induced as a result of the bending.

This will be a transformative idea as one can enable routing and networking on the surface in infrared, to send the information from one point to another in an efficient wave;

for instance, to collect the light from space and communicate on the surface. Also, we note that the design dimensions can be scaled according to operation wavelength from THz to NIR regions of spectrum.

V. Conclusion

We developed and characterized a plasmonic unit cells for graded index material applications. The unit cell is a metallic patch on a grounded substrate. We then demonstrated the application of such unit cell for design of flat-graded index structures for guiding and radiation waves at infrared range. A high gain high efficiency flat-graded index antenna is presented at infrared range. Also, we demonstrated a flat surface waveguide and we thoroughly investigated propagation properties and obtained values for the associated propagation loss. Then, we proposed a new feeding scheme for graded index holograms using the flat surface waveguide. This feeding system makes a full planar hologram metasurface possible. Also, routing of the waves on the surface is demonstrated using a bend structure.

References

[1] D. W. Prather, J. N. Mait, M. S. Mirotznik, and J. P. Collins, "Vector-based synthesis of finite aperiodic subwavelength diffractive optical elements," *J. Opt. Soc. Amer. A*, vol. 15, pp. 1599–1607, 1998.

[2] Z. L. Mei, J. Bai, and T. J. Cui, "Gradient index metamaterials realized by drilling hole arrays," *J. Phys. D: Appl. Phys.*, vol. 43, p. 055404, 2010.

[3] B. Good, P. Ransom, S. Simmons, A. Good, and M. S. Mirotznik, "Design of graded index flat lenses with integrated antireflective properties," *Microw. Opt. Technol. Lett.*, vol. 54, pp. 2774–2781, 2012.

[4] U. Levy, M. Nezhad, H.-C. Kim, C.-H. Tsai, L. Pang, and Y. Fainman, "Implementation of a graded-index medium by use of subwavelength structures with graded fill factor," *J. Opt. Soc. Amer. A*, vol. 22, pp. 724–733, Apr. 2005.

[5] F. M. Huang, N. Zheludev, Y. Chen, and F. J. G. de Abajo, "Focusing of light by a nanohole array," *Appl. Phys. Lett.*, vol. 90, pp. 091119–3, 2007.

[6] L. Verslegers, P. B. Catrysse, Z. Yu, J. S. White, E. S. Barnard, M. L. Brongersma, and S. Fan, "Planar lenses based on nanoscale slit arrays in a metallic film," *Nano Lett.*, vol. 9, pp. 235–238, Jan. 2009.

[7] B. Memarzadeh and H. Mosallaei, "Array of planar plasmonic scatterers functioning as light concentrator," *Opt. Lett.*, vol. 36, pp. 2569–2571, 2011.

[8] N. Yu, P. Genevet, M. A. Kats, F. Aieta, J.-P. Tetienne, F. Capasso, and Z. Gaburro, "Light propagation with phase discontinuities: Generalized laws of reflection and refraction," *Science*, vol. 334, pp. 333–337, 2011.

[9] M. Farmahini-Farahani and H. Mosallaei, "Birefringent reflectarray metasurface for beam engineering in infrared," *Opt. Lett.*, vol. 38, pp. 462–464, 2013.

[10] T. Niu, W. Withayachumnankul, B. S. Y. Ung, H. Menekse, M. Bhaskaran, S. Sriram, and C. Fumeaux, "Experimental demonstration of reflectarray antennas at terahertz frequencies," *Opt. Exp.*, vol. 21, pp. 2875–2889, 2013.

[11] A. Pors, O. Albrektsen, I. P. Radko, and S. I. Bozhevolnyi, "Gap plasmon-based metasurfaces for total control of reflected light," *Sci. Rep.*, vol. 3, 2013.

[12] H. Ditlbacher, J. Krenn, G. Schider, A. Leitner, and F. Aussenegg, "Two-dimensional optics with surface plasmon polaritons," *Appl. Phys. Lett.*, vol. 81, pp. 1762–1764, 2002.

[13] T. Zentgraf, Y. Liu, M. H. Mikkelsen, J. Valentine, and X. Zhang, "Plasmonic Luneburg and Eaton lenses," *Nat. Nano*, vol. 6, pp. 151–155, 2011.

[14] A. Vakil and N. Engheta, "Fourier optics on graphene," *Phys. Rev. B*, vol. 85, p. 075434, 2012.

[15] S. Sun, Q. He, S. Xiao, Q. Xu, X. Li, and L. Zhou, "Gradient-index metasurfaces as a bridge linking propagating waves and surface waves," *Nat. Mater.*, vol. 11, pp. 426–431, 2012.

[16] K. Crozier, A. Sundaramurthy, G. Kino, and C. Quate, "Optical antennas: Resonators for local field enhancement," *J. Appl. Phys.*, vol. 94, pp. 4632–4642, 2003.

[17] Lumerical Solutions, Inc. [Online]. Available: http://www.lumerical.com/tcad-products/fdtd/

[18] Q. Song, S. Campione, O. Boyraz, and F. Capolino, "Silicon-based optical leaky wave antenna with narrow beam radiation," *Opt. Exp.*, vol. 19, pp. 8735–8749, Apr. 2011.

[19] B. H. Fong, J. S. Colburn, J. J. Ottusch, J. L. Visher, and D. F. Sievenpiper, "Scalar and tensor holographic artificial impedance surfaces," *IEEE Trans. Antennas Propag.*, vol. 58, no. 10, pp. 3212–3221, Oct. 2010.

[20] A. M. Patel and A. Grbic, "A printed leaky-wave antenna based on a sinusoidally-modulated reactance surface," *IEEE Trans. Antennas Propag.*, vol. 59, no. 6, pp. 2087–2096, Jun. 2011.

[21] M. ElSherbiny, A. E. Fathy, A. Rosen, G. Ayers, and S. M. Perlow, "Holographic antenna concept, analysis, and parameters," *IEEE Trans. Antennas Propag.*, vol. 52, no. 3, pp. 830–839, Mar. 2004.

[22] A. Oliner and A. Hessel, "Guided waves on sinusoidally-modulated reactance surfaces," *IEEE Trans. Antennas Propag.*, vol. 7, no. 5, pp. 201–208, Dec. 1959.

[23] E. Snitzer, "Cylindrical dielectric waveguide modes," *J. Opt. Soc. Amer.*, vol. 51, pp. 491–498, 1961.

[24] E. A. Marcatili, "Dielectric rectangular waveguide and directional coupler for integrated optics," *Bell Syst. Tech. J.*, vol. 48, pp. 2071–2102, 1969.

[25] M. Adams, *An Introduction to Optical Waveguides*. Chichester, U.K.: Wiley, 1984.

[26] D. J. Gregoire and A. V. Kabakian, "Surface-wave waveguides," *IEEE Antennas Wireless Propag. Lett.*, vol. 10, pp. 1512–1515, Dec. 2011.

[27] R. Quarfoth and D. Sievenpiper, "Artificial tensor impedance surface waveguides," *IEEE Trans. Antennas Propag.*, vol. 52, no. 7, pp. 830–839, Jul. 2013.

Mohsen Farmahini-Farahani (S'06) received the B.Sc., M.Sc., and Ph.D. degrees in electrical engineering from the Iran University of Science and Technology, Tehran, Iran, University of Tehran, Tehran, and Northeastern University, Boston, MA, USA, in 2006, 2009, and 2014, respectively.

His past research interests include the area of novel plasmonic and passive components in THz and optics, antenna design, inverse scattering problems in electromagnetics, optimization in electromagnetics, spatial power combining and passive and active microwave circuits.

He is currently with the Antenna Department, Qualcomm Research Center, San Diego, CA, USA, working on designing novel antennas for different telecommunications applications.

Hossein Mosallaei (S'98–SM'02) received the B.Sc. and M.Sc. degrees in electrical engineering from Shiraz University, Shiraz, Iran, and the Ph.D. degree in electrical engineering from the University of California, Los Angeles, CA, USA, in 1991, 1994, and 2001, respectively.

From 2002 to 2005, he was a Research Scientist in EECS Department, University of Michigan, Ann Arbor, MI, USA. He is currently an Associate Professor of electrical and computer engineering in the College of Engineering, Northeastern University, Boston, MA, USA. His research interests include theory and computation of electromagnetic and optical metamaterials. He has authored and coauthored more than 150 technical journal articles and conference papers.

Dr. Mosallaei is a Full Member of the International Union for Radio Science (URSI), and a Member of the American Association for the Advancement of Science. He is the holder of one U.S. patent. He was the recipient of student prize paper awards in AP-S 2000, 01, 03, and 05 along with his students, URSI Young Scientist Award in 2001, and RMTG Award in 2002. His student won the Northeastern Dissertation-Writing Fellowship Award in 2010.